Materials Research. 2023; 26: e20220110
DOI: https://doi.org/10.1590/1980-5373-MR-2022-0110

A Strength Behavior Approach for 3Y-TZP Ceramics Dental Implants Based on Finite Element Simulations

Pedro Araújo da Costa Ward[a], Fernando Araújo da Costa Ward[a], Thielly Machareth Ward[b], Claudinei dos Santos[a,b]*, Rodrigo Xavier de Freitas[c], Luciano Pessanha Moreira[a]

[a]*Universidade Federal Fluminense (UFF), Escola de Engenharia Industrial Metalúrgica de Volta Redonda (EEIMVR), CEP 27255-125, Volta Redonda, RJ, Brasil.*
[b]*Universidade do Estado do Rio de Janeiro (UERJ), Faculdade de Tecnologia de Resende (FAT), CEP 27537-000, Resende, RJ, Brasil.*
[c]*Centro Universitário de Volta Redonda (UniFOA), CEP 27240-560, Volta Redonda, RJ, Brasil.*

Received: March 08, 2022; Revised: January 03, 2023; Accepted: January 24, 2023

This study is based on the numerical simulation of the mechanical response of yttrium-stabilized zirconia ceramic (3Y-TZP) dental implants as a function of their intrinsic geometry and masticatory loads. Samples (n=20) of 3Y-TZP ceramics were compacted, sintered at 1500 °C - 2h, and characterized by relative density, X-Ray diffraction (XRD), and scanning electron microscopy (SEM). The elastic parameters (modulus of elasticity and Poisson ratio), used in the numerical simulations, were measured by the Impulse Excitation Technique, and the bending strength was obtained using piston-on-three-balls testing. An authorial implant design and, comparatively, commercial implant CAD models were used in this study as an initial geometry of dental implant in a typical adult mandible anatomy. From CAD and CAE techniques, finite element models were generated for all implant geometries. Loading cases were considered based on different intensities (100N to 500N) and orientation angles (45° or 90°) to reproduce the human masticatory efforts. The numerical predictions were compared with finite element simulations of gold-standard titanium-based implants. The investigated 3Y-TZP sintered ceramics presented high densification (> 99%), with a microstructure formed by submicron equiaxed tetragonal zirconia grains. The 3Y-TZP average bending strength obtained from piston-on-three-balls testing is 1192 ± 99 MPa. For both dental implant geometries, the zirconia implants showed average strength of less than 550 MPa, which, in turn, is independent of the masticatory load value or orientation angle. All finite element predictions are 50% inferior to the corresponding measured flexural strength values and preliminarily enable the 3Y-TZP ceramics for dental implant applications without fracture risk.

Keywords: *Dental implants, 3Y-TZP ceramics, flexural strength, numerical simulation, finite element method.*

1. Introduction

Bioceramics based on Yttrium-stabilized tetragonal zirconia polycrystals (Y-TZP) are very attractive to dentistry applications due to their biocompatibility, high fracture toughness, strength, strong hardness, and low bacterial plaque adhesion[1]. Zirconia stabilized with 3 mol.% Y_2O_3 (3Y-TZP) exhibits high flexural strength (1000 MPa) and good fracture toughness (7 to 9 MPa m$^{1/2}$). The improved 3Y-TZP mechanical properties are usually attributed to tetragonal to monoclinic zirconia transformation (*t→m*)[2-5] and consequent microcracking and toughening mechanisms. This is a consequence of the volumetric expansion and shear stress component associated with the *t→m* transformation, leading to crack propagation inhibition around the crack tip. These two mechanisms are associated, promoting the high strength of Yttria-stabilized tetragonal zirconia (Y-TZP) ceramics. A third mechanism is a ferroelastic effect, also known as ferroelasticity. This effect arises from the mechanical commutation of two differently oriented domains under an applied load, exceeding the critical material stress. This mechanism was studied in detail in sintered Y-TZP using in-situ neutrons diffraction during mechanical compression tests[6,7].

In the last years, the 3Y-TZP bioceramics have been used as dental implants, presenting a market growing nearly 12% per year[8]. The threaded design to assure the dental implant mechanical anchorage at the bone is one of the main challenges to prosthetics. This design is more critical for ceramic materials due to stress concentrations at the sharp edges[9]. Nowadays, more than 15 companies worldwide produce zirconia dental implants, each with its processing, design, and surface to promote osseointegration[10]. Also, different *in vitro* and *in vivo* investigations have established the biocompatibility and osteogenic potential of Zirconia-based implants[11]. Nevertheless, in compromised patient conditions (inadequate bone quality/quantity, aged and diabetic patients), early establishment and long-term maintenance of osseointegration at the bone-implant interface, and soft-tissue

*e-mail: claudineisvr@gmail.com

integration at the transmucosal region of dental implants, may be inadequate[12].

The present work aims to evaluate the mechanical behavior of 3Y-TZP dental implants compared to traditional titanium-based implants used in the third molar. For this purpose, numerical simulations are performed using the finite element method of an implant model inserted only in a mandible segment composed of two bone layers, cortical and trabecular[13-15]. The third molar region was chosen since this area has conditions of masticatory efforts similar to the first and second molars. Also, this region presented greater technical ease for performing the computer simulations[16]. The finite element analysis at these critical regions helps determine the local stress concentration fields and the resulting average strength under representative masticatory loading conditions.

2. Experimental and Numerical Procedures

2.1. Processing and characterization of 3Y-TZP ceramics

Zirconia powder containing 3 mol.% Y_2O_3 (TOSOH, 3YSB-E, Japan) was used in this study. Different 3Y-TZP specimens, discs of Ø15 x 1.5 mm (n=25) and bars 50 x 5 x 4 mm^3 (n = 4), were firstly cold uniaxial pressed at 150 MPa and then sintered at 1500 °C - 2h, using a $MoSi_2$ furnace (MAITEC® F1650, Brazil), with a heating rate of 2°C / min. The cooling rate adopted in this work was 5° C/min to room temperature.

After sintering, the surfaces of the specimens were sanded with SiC sandpaper (Buehler Ltd) with 600, 800, and 1200 granulation, undercooling, and manual pressing at 200 rpm with a South Bay Technology, Inc (USA) 900 model polisher. Next, the specimens were polished with diamond pastes of 3, 1, and 0.25 μm (Arotec, São Paulo, Brazil), washing the samples after each stage.

The crystalline phases were identified using an Empyrean diffractometer (Malvern Panalytical, Worcestershire - UK) equipped with a Cu-Kα radiation source. The scanning was accomplished at the 2θ range between 20 and 90°, with a 0.03° step width and 100 s exposure time. The Rietveld refinement technique was used using tetragonal zirconia, t-ZrO_2 (P42/nmc), monoclinic zirconia, m-ZrO_2 (P21/c), and cubic zirconia, c- ZrO_2 (Fm-3m) as possible crystalline structures.

The apparent density of the sintered material was measured according to ASTM B962-15, using an Ohaus electronic scale, Discover model, with ± 0.0001g precision. The relative density was obtained by adopting 6.05 g/cm^3 as theoretical density.

The zirconia specimens were submitted to heat treatment at 1400 °C for 15 min (25°C/min) for microstructural revelation. The polished surfaces have been coated with gold using a Coater Sputter Emitech K550 (Quorum Technologies – UK) with 30mA for 2min and analyzed using a scanning electron microscope (JEOL® FEG JSM 7100FT, Japan) with SE and 15 kV/WD 10 mm detector.

The elastic parameters (modulus of elasticity and Poisson ratio), used in the numerical simulations, were measured by the Impulse Excitation Technique, IET, in a apparatus model-Sonelastic®, ATCP- São Carlos, Brazil, using discs with final dimensions of 12.5 mm in diameter and 1.3 mm thick to obtain the modulus of elasticity, and bars (45 x 4 x 3 mm^3), to determine the Poissin ratio, following the recommendations of the ASTM E1876-15 standard[17].

Furthermore, the biaxial flexural strength was evaluated with the piston-on-three-balls (P-3B) testing procedure[18], using a universal testing machine (EMIC® 1000 INSTRON-Group, Brazil) under a constant cross-head speed of 0.5 mm/min. Experimental details of the P-3B testing are given elsewhere[19].

2.2. Dental implant numerical simulations

A scanned adult man mandible 3D model from CAM software was initially imported on ".stl" format and simplified using the CATIA V5 software. Figure 1 shows only the 3rd molar region section used for the finite element mesh generation, which is the region most affected by masticatory loads. Due to the complex human mandible geometry, the primarily obtained geometry is too complicated for finite element computational analysis. Table 1 shows the mechanical properties difference between cortical bone[20] (external bone layer) and trabecular[20] (internal bone layer), titanium[21] and ZrO_2 - 3%Y_2O_3 properties used as dental implants. All properties were considered assuming linear isotropic elasticity described by Hooke's law. The Mohr-Coulomb and von Mises isotropic yield criterion were adopted to describe the mechanical behavior of the ceramics and titanium implant materials, respectively.

Two CAD-based dental implants were built. First, a commercial model based on the Straumann® commercial implant is depicted in Figure 2 with varying diameters of Ø 4.1 – 4.8 mm and 0.8 mm thread pitch. Second, an authorial model was obtained from a geometry modification with a cylindrical head instead of a conical shape.

A new geometry was proposed, considering cylindrical implants as opposed to conical implants, aiming exclusively to evaluate the mechanical conditions in a comparative way, after a protocol period of osseointegration/healing,

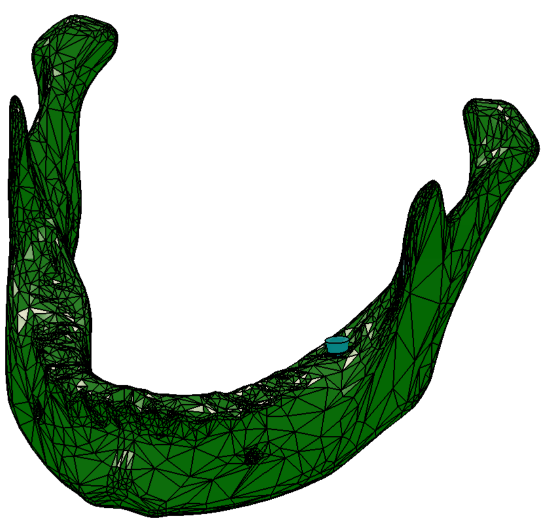

Figure 1. Mandible geometry of an adult male with a commercial implant model.

Table 1. Mechanical properties of materials used in numerical simulations[20,21].

Material	Young's Modulus (MPa)	Adopted Young´s Modulus (MPa)	Poisson's ratio	Bending Strength (MPa)	Compression strength (MPa)
ZrO_2 - 3%Y_2O_3	195300 ± 4000	195300	0.31	965.3	2000
Cortical bone	7000 ~ 30000	30000	0.33	-	-
Trabecular bone	50 ~ 500	500	0.33	-	-
Titanium	110000	110000	0.35	550	-

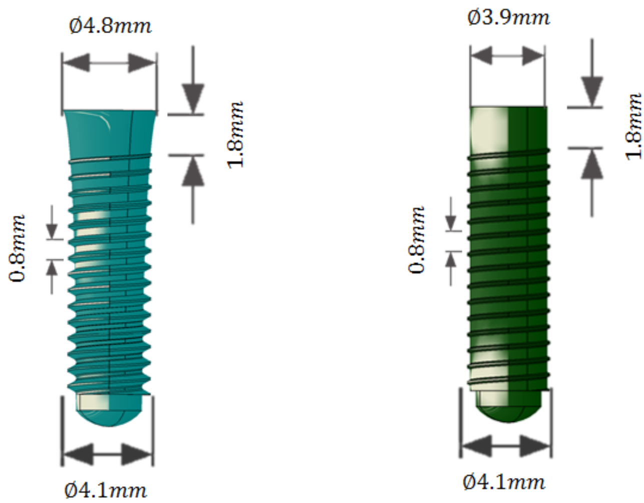

Figure 2. a) Commercial implant geometry; b) Authorial implant geometry adapted from the results obtained from the commercial implant geometry.

without considering the initial post-surgical effects of stress distributions in the bone-implant system. The simulations considered implants with balanced stress in the implantation region, without postoperative implantation effects, and where compressive effects of installation, or misfit due to differences between pre-hole diameter and implant diameter and bone stiffness may occur.

In both implant geometry cases and investigated materials (zirconia or titanium), a concentrated load of 100 N or 500 N was applied with an orientation angle of 0° or 45° to the implant longitudinal axis, as shown in Figure 3.

The finite element modeling was performed with the ABAQUS code. The solid tetrahedral first-order element with 4-four nodes (C3D4) was used for the mesh discretization. The mandible element sizes equal 0.5 mm, whereas the implant elements have 0.25 mm. A more refined mesh was chosen for the implants, focusing on the proposed finite element modeling. The proposed generated mesh is depicted in Figure 3.

The implants have 11,146 nodes, while the mandible section mesh (trabecular and cortical bone) has 31,200 nodes. The encastre boundary condition was considered on the sectioned mandible surfaces to reduce the computational processing time. On the other hand, the implant is fixed to the mandible using the tie contact option under frictionless conditions. The contact conditions can also be visualized in Figure 4. All simulations were run in a dual-processor workstation Intel Xeon 5690 3.47 GHz, 24 cores with 32 Gb RAM.

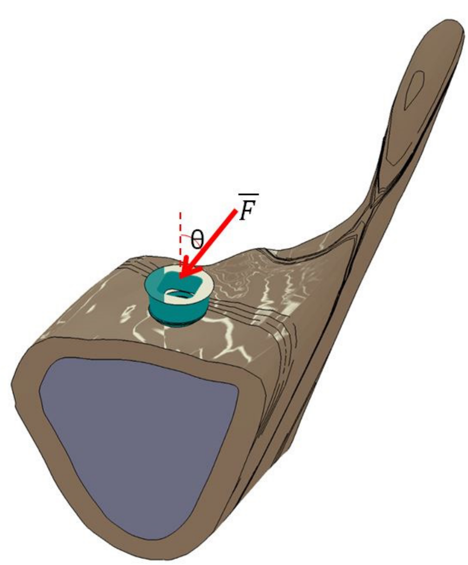

Figure 3. Sectioned mandible close to the third molar with a representative applied masticatory load (F) used on the commercial implant geometry at an orientation angle (θ).

3. Results and Discussion

Figure 5 presents the XRD pattern of the sintered specimens. The 3Y-TZP zirconia indicates only ZrO_2 peaks with tetragonal (74%) and cubic (26%) structures, as obtained in the previous work[22]. In addition, Figure 5b shows an SEM micrograph representative of 3Y-TZP specimens after 1500 °C- 2 h sintering. It is possible to notice semispherical grains with micrometric size morphology. The presence of the pores was not observed, thus, indicating a high densification degree obtained after the sintering, as measured by the Arquimedes principle, which presents a relative density near 99.4 ± 0.2%. There are two distinct grain size classes of 3Y-TZP specimens. One group has grain sizes inferior to 0.4 μm and the other close to 1.0 μm. From the X-ray patterns, they correspond to the phases containing tetragonal and cubic structures (bigger grains), respectively. Previous works investigated the migration of Y^{+3} to some preferred ZrO_2 grains, increasing the stabilization trend of the ZrO_2-cubic phase and its growth rate compared to ZrO_2-tetragonal grains[23-25].

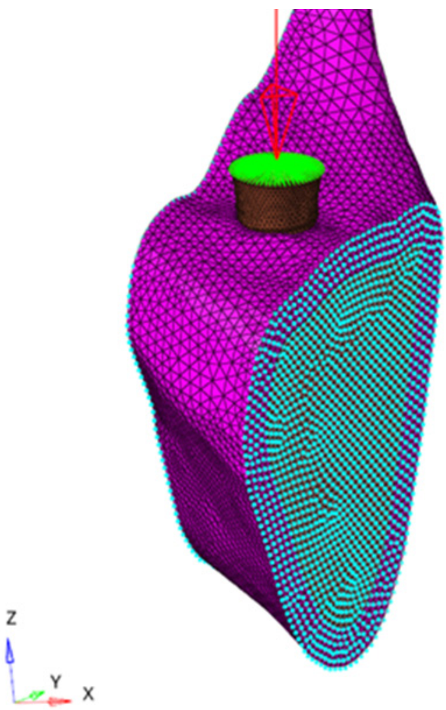

Figure 4. Finite element mesh and boundary conditions.

The measured elastic parameters were presented in Table 1, and presented a modulus of elasticity of 195 ±4 GPa, for values measured in 15 sintered samples, indicating little statistical variation, while the measured poisson ratio was 0.31, with no statistical variation detected by the equipment used for measurement, demonstrating the homogeneity of the ceramic samples developed in this study.

The average flexural strength values obtained from the P-3B testing equal 1192 ± 99 MPa, and the Weibull distribution plot is shown in Figure 6. It is possible to notice that 3Y-TZP specimens present a superior Weibull module, m = 14.7. The 3Y-TZP failure probability is lower than 70% for the stress level of 1192 MPa. Thus, the failure probability determined by Weibull statistics is acceptable for stress levels lower than this. For the 20 specimens experimental group, it is worth highlighting that they all showed flexural strength above 900 MPa.

Figure 7 shows the numerical predictions of the 3Y-TZP and titanium implants obtained for the maximum principal stress (σ_1) contour plots (MPa) from the higher loading condition (500 N) with an orientation angle of 45° to the implant longitudinal axis. The corresponding numerical results determined from these models for the minimum principal stress (σ_3) contour plots (MPa) are depicted in Figure 8. As observed, the loading effect on the stress components in the mandible is inferior compared with the implant. Thus, further predictions are shown only on the isolated implant for the failure risk analysis.

Table 2 resumes the peak values of the maximum and minimum principal stress components determined from the results in the isolated commercial and authorial implants shown in the right column of Figure 7. The commercial and authorial implant designs, respectively, provided maximum principal stress for the 3Y-TZP (respective titanium) 261.20 MPa (263.60 MPa) and 382.46 MPa (523.03 MPa). In the same manner, the peak values from the results shown in Figure 8 corresponding to the minimum principal stresses in the commercial and authorial implant designs, respectively, for the 3Y-TZP ceramics (respective titanium) are – 743.04 MPa (826.27 MPa) and – 613.12 MPa (586.50 MPa). Conversely, it is worth observing from Figures 7 and 8 that the maxima (respective minima) peak values are located at the corners of the implant base (respective at the outer surface of the first screw threads) for both commercial and authorial designs

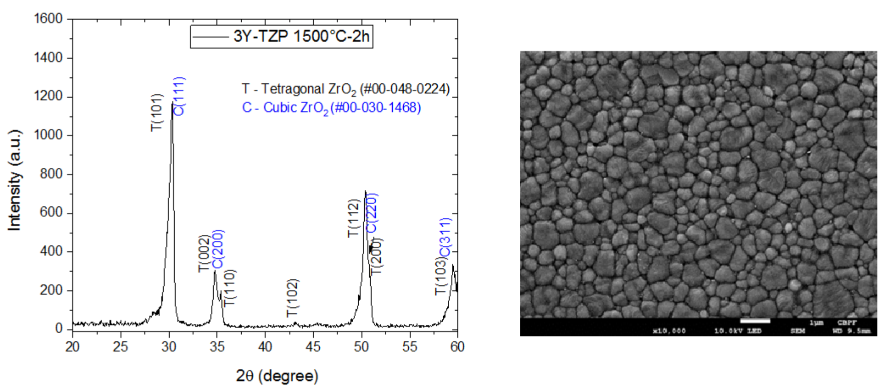

Figure 5. a) X-ray diffractogram; b) SEM micrograph of a 3Y-TZP sample sintered at 1500 °C-2h.

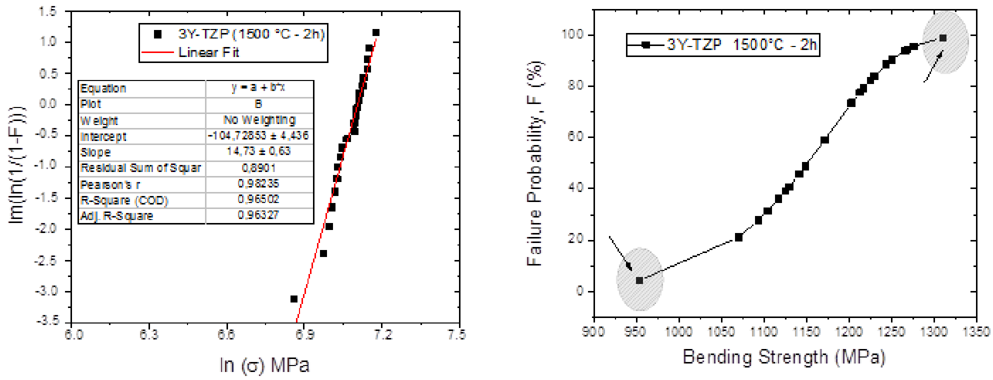

Figure 6. (a) Weibull distribution and (b) failure probability as a function of the flexural strength of 3Y-TZP ceramics sintered at 1500 °C - 2h.

Table 2. Numerical predictions of the peak maxima (σ_1) and minima (σ_3) principal stress components obtained from the 3Y-TZP and titanium implants for the higher loading condition (500 N) at 45° to the implant axis.

Peak stress (MPa)	ZrO2 - 3 mol.%Y2O3		Titanium	
	Commercial	Authorial	Commercial	Authorial
σ_1	261.20	382.47	263.60	523.03
σ_3	-734.04	-613.12	-826.27	-535.03

of either 3Y-TZP ceramics and titanium implant materials. The applied concentrated compression loading (500 N) is oriented at 45° to the implant longitudinal axis, which, in turn, is decomposed into normal and tangential forces acting in these two implant regions.

Figure 6 shows the Weibull distribution and failure probability of the investigated 3Y-TZP ranging from 950 MPa to approximately 1310 MPa. Comparing the lowest bending strength amongst all specimens (close to 950 MPa) with the highest peak value of the maximum principal stress determined from the numerical simulations for the authorial implant design (382.46 MPa) indicates a high safety factor for the $ZrO_2 – 3mol.\%Y_2O_3$ ceramics. This result is also substantiated by the corresponding peak minimum principal stress obtained for the commercial implant design (– 743.04 MPa) compared to the higher yield strength under uniaxial compression of the 3Y-TZP ceramics. This comparison highlights the ZrO_2 - 3 mol.%Y_2O_3 ceramics mechanical reliability, combined with the biological properties, represent a feasible alternative to titanium-based implants. Furthermore, it should be remarked that the toughening mechanisms were not considered in the finite element modeling. Thus, the practical use of 3Y-TZP ceramics would provide high fracture toughness, strength resistance, and improved hardness.

In the finite element analysis, the risk of failure of the investigated ceramic material is described by the Mohr-Coulomb yield criterion, which can be stated as[26].

$$\left(\frac{\sigma_1}{\sigma_{ut}} + \frac{\sigma_3}{\sigma_{uc}}\right) \leq 1 \tag{1}$$

where σ_1 and σ_3 are the maximum and minimum principal stresses whereas σ_{ut} and σ_{uc} denote the ultimate yield strength under uniaxial tension and compression, respectively. The Mohr-Coulomb failure criterion is more suitable for brittle materials for which the compressive yield strength is higher than the tensile yield strength, as is the case of the 3Y-TZP ceramics[27]. For simplicity, the term in parenthesis in Equation 1 is called MC and can be viewed as the risk of failure as it approaches unity.

On the other hand, one may use classical ductile failure criteria to describe the mechanical behavior of the titanium implant material. Here, the von Mises yield criterion is adopted as

$$\frac{1}{2}\left[\left(\frac{\sigma_1 - \sigma_2}{\sigma_{ut}}\right)^2 + \left(\frac{\sigma_2 - \sigma_3}{\sigma_{ut}}\right)^2 + \left(\frac{\sigma_3 - \sigma_1}{\sigma_{ut}}\right)^2\right] \leq 1 \tag{2}$$

where σ stands for the intermediate principal stress. In the same way, the left-hand side of Equation 2 is termed vonMises, representing the risk of failure as it is close to unity. It should be remarked that both Mohr-Coulomb and von Mises yield criteria are available in the ABAQUS finite element code and, accordingly, the corresponding risk of failure measures defined by Equations 1 and 2, respectively, are obtained as a post-processing step from the principal stress components (σ_1,σ_2,σ_3) by defining user output field variables (MC and vonMises) together with the values of the uniaxial tension ultimate yield strength (σ_{ut}) and uniaxial tension ultimate yield strength (σ_{uc}).

Figures 9 and 10 show the numerical predictions in the commercial and authorial implant designs, which were obtained as a function of the loading values (100 N and 500N) and axis loading orientation angle (90° and 45°). These finite element results were obtained from the adopted failure criteria as dimensionless scalar (invariant) measures of the Mohr-Coulomb and von Mises yield criteria, defined by Equations 1 and 2, respectively,

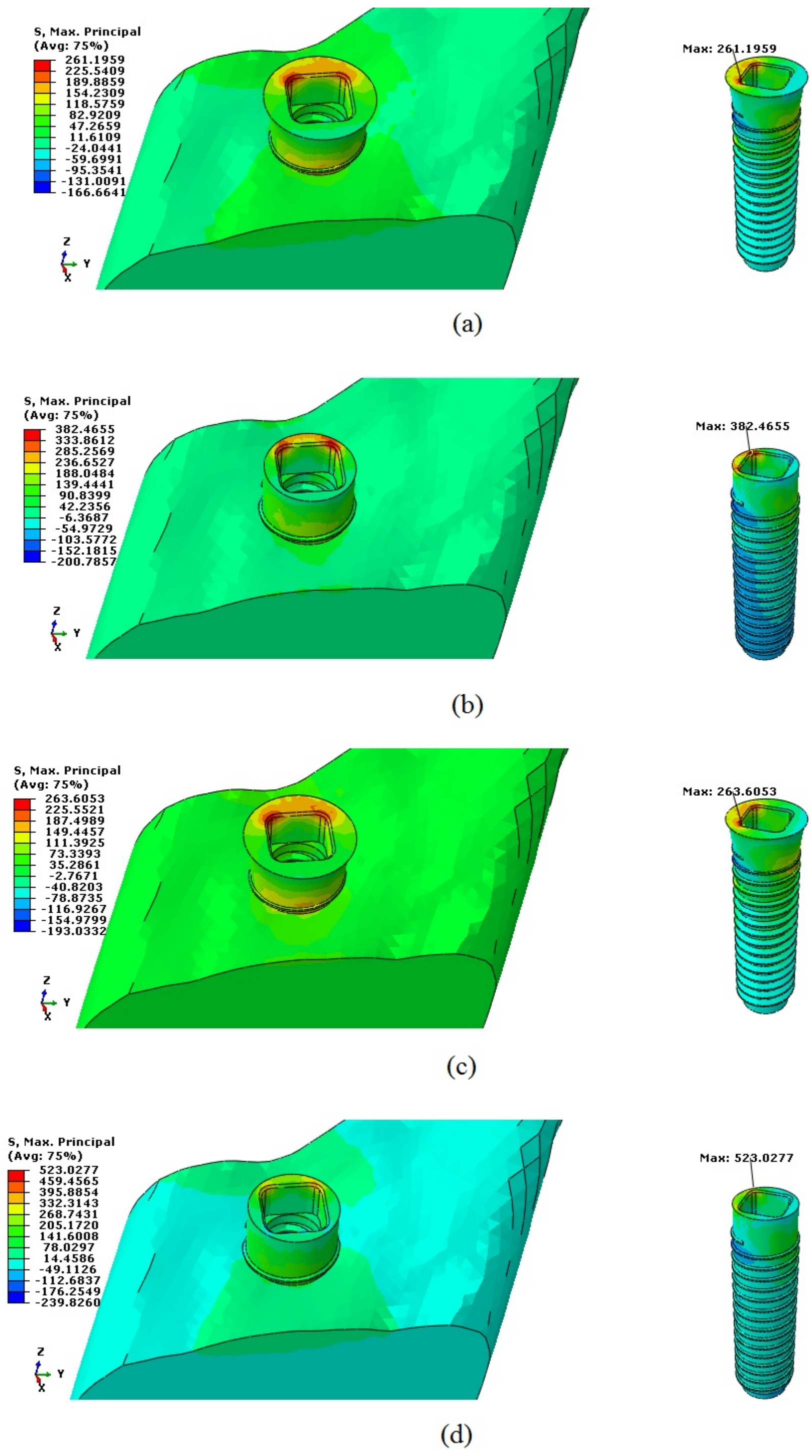

Figure 7. Maximum principal stress (σ_1) contour plots (MPa) of the implants submitted to a masticatory axial loading 500 N at 45° to the longitudinal axis: 3Y-TZP ceramics (a) commercial and (b) authorial; titanium (c) commercial and (d) authorial.

which indicate the risk of failure as the corresponding failure factors (MC and vonMises) approach unity. As the normal axial load increases, one can observe from Figure 9 that the risk of failure is more significant in both titanium-based implants and that both implant materials offer failure factor values inferior to 1. For the oblique loadings, the titanium-based implants show considerable failure risk under the higher load (500 N) for both the commercial (vonMises = 1.004) and authorial (vonMises = 0.847) designs, as shown in Figures 10f and 10h, respectively. Conversely, the 3Y-TZP ceramic implants failure factors increased from 0.196 (500 N/90°) to 0.253 (500 N/45°) and 0.167 (500 N/90°) to 0.325 (500 N/45°) for the commercial

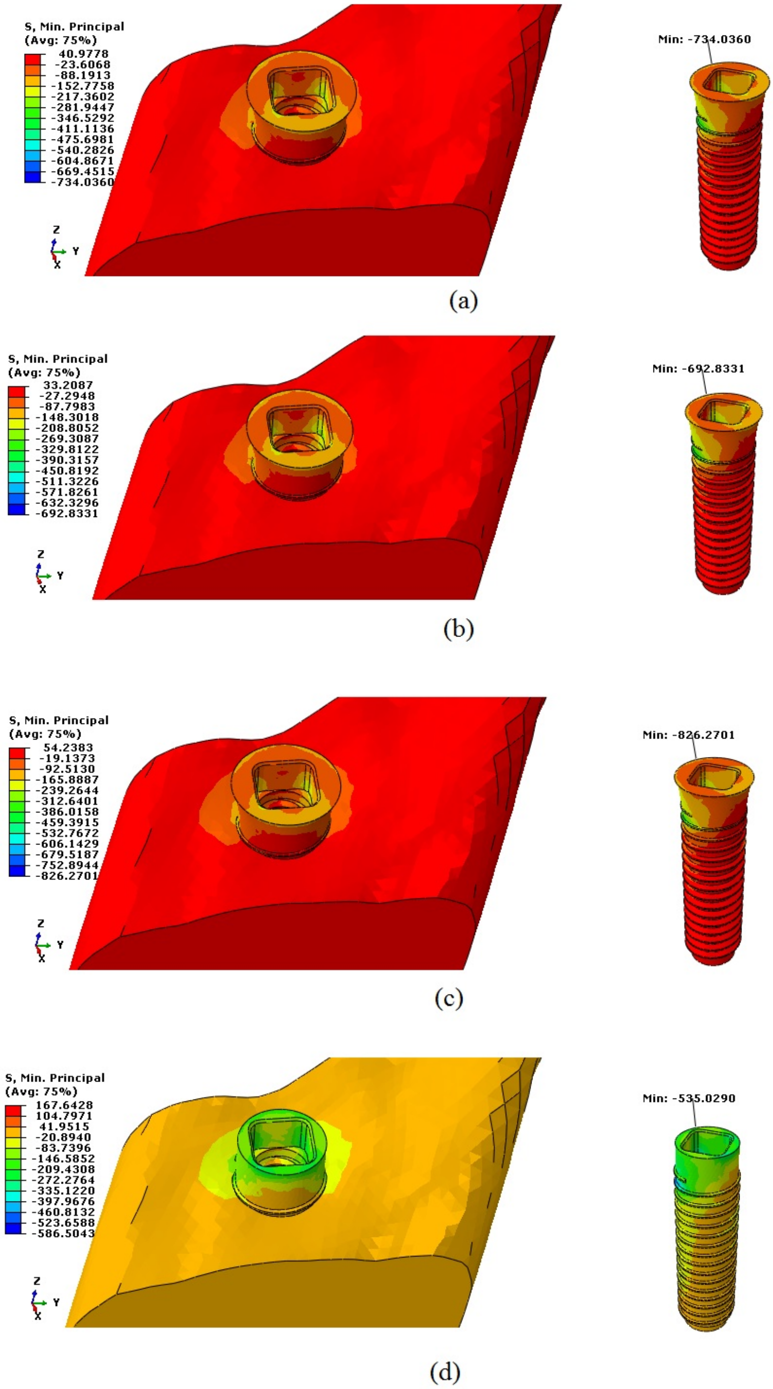

Figure 8. Minimum principal stress (σ_3) contour plots (MPa) of the implants submitted to a masticatory axial loading 500 N at 45° to the longitudinal axis: 3Y-TZP ceramics (a) commercial and (b) authorial; titanium (c) commercial and (d) authorial.

and authorial designs, respectively. Tables 3 and 4 summarize the numerical predictions of the risk of failure determined as a function of loading conditions for the titanium and 3Y-TZP, respectively.

Yttrium-stabilized zirconia (Y-TZP) ceramics present a flexural strength loss due to aging, a consequence of hydrothermal degradation in aqueous environments[28-30], or when submitted to cyclic loading as fatigue. Thus, these parameters must be considered in the design of the geometry of ceramic implants, aiming to improve the reliability of this material. In a recent study[31], 3Y-YZP ceramics were tested in different experimental groups before and after hydrothermal degradation. The results showed around 12% of flexural strength loss caused by *tetragonal* → *monoclinic*

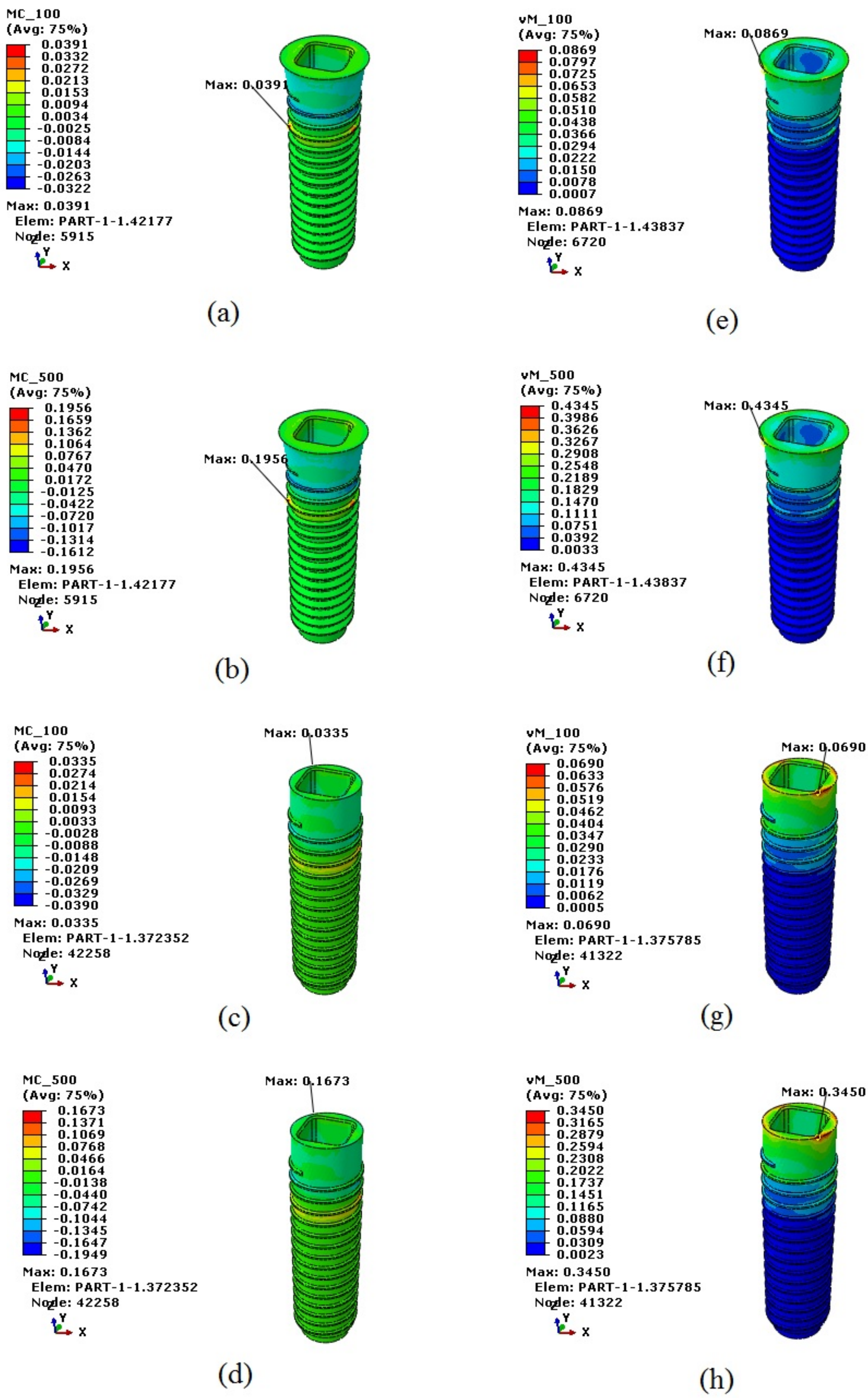

Figure 9. Numerical predictions of the contours values of the risk of failure determined from masticatory axial loads at 90º to the implant longitudinal axis for the 3Y-TZP ceramics: commercial (a) 100 N and (b) 500 N and authorial designs: (c) 100 N and (d) 500 N (right column). Titanium-based implants (left column): commercial (e) 100 N and (f) 500 N and authorial designs: (g) 100 N and (h) 500 N.

precocious transformation, with static average flexural strength (4-points) results close to 940 MPa. The fatigue behavior analyses on the aged samples (degraded) group in an autoclave (134 °C - 5h, which corresponds to 30 years in the oral environment) showed that the cyclic fatigue strength limit of these degraded 3Y-TZP ceramics was 550 MPa,

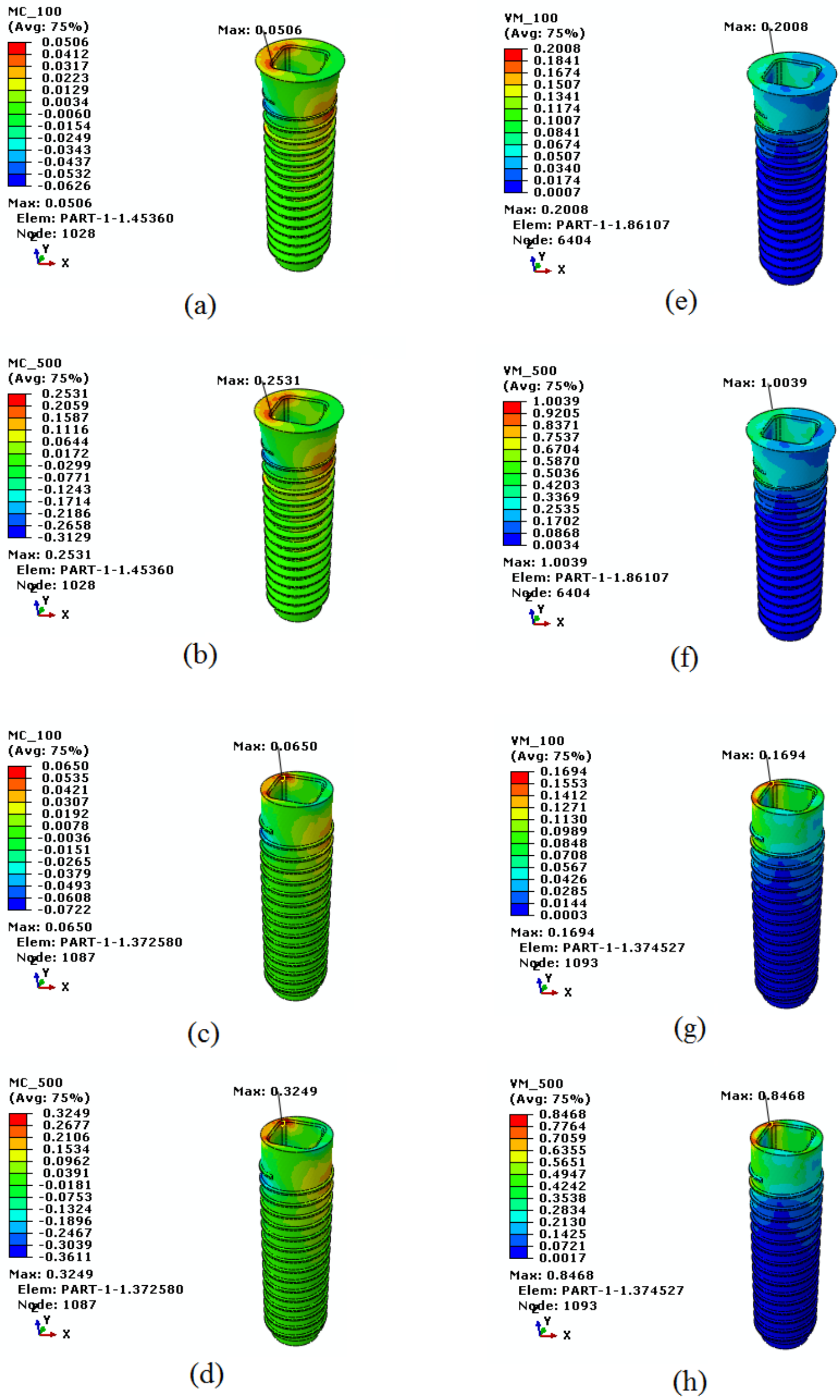

Figure 10. Numerical predictions of the contours values of the risk of failure determined from masticatory axial loads at 45° to the implant longitudinal axis for the 3Y-TZP ceramics: commercial (a) 100 N and (b) 500 N and authorial designs: (c) 100 N and (d) 500 N (right column). Titanium-based implants (left column): commercial (e) 100 N and (f) 500 N and authorial designs: (g) 100 N and (h) 500 N.

which indicates that, even at the most severe conditions these works developed implants that successfully resist as dental implants. It is worth mentioning that these studies are still preliminary investigations. Therefore, ceramic prototypes must be mechanically developed and tested for definitive use.

Table 3. Numerical predictions of the risk of failure (von Mises criterion) for the titanium implants as a function of the loading case.

Implant type	Material	100 N	100 N (45°)	500 N	500 N (45°)
Commercial	Titanium	0.0869	0.2008	0.4345	1.0038
Authorial		0.0690	0.1964	0.3450	0.8468

Table 4. Numerical predictions of the risk of failure (Mohr-Coulomb criterion) for the titanium implants as a function of the loading case.

Implant type	Material	100 N	100 N (45°)	500 N	500 N (45°)
Commercial	ZrO_2 - 3 mol.%Y_2O_3	0.0391	0.0506	0.1956	0.2531
Authorial		0.0335	0.0650	0.1673	0.3249

4. Conclusions

The prototype of the new implant authorial design indicated that under the severe masticatory loading evaluated (500 N at 45° to the implant axis), the maximum principal stress (respective minimum principal stress) is equal to 382.46 MPa (respective – 613.12 MPa) and 523.03 MPa (respective – 535.03 MPa) for the 3Y-TZP ceramics and titanium materials, respectively. Bearing in mind that the measured average flexural strength of the investigated 3Y-TZP ceramic is 1190 MPa, ranging from 950 up to 1310 MPa, the potential use of the lowest representative stress level (950 MPa) indicates a safety window for its practical use in dental implants. This outcome is corroborated by the risk of failure analysis results performed in both commercial and authorial implant designs based on the Mohr-Coulomb (3Y-TZP) and von Mises (titanium) criteria. Thus, based on these preliminary experimental-numerical findings, the 3Y-TZP ceramics shows the potential use to replace titanium in actual dental implant manufacturing. However, possible stress distribution changes in the implant/osseomandibular region originating from changes in implant geometry in the surgical and post-surgical stages should be explored in future work.

5. Acknowledgments

This research was funded by Coordenação de Aperfeiçoamento de Pessoal de Nível Superior (CAPES, Brazil) – Finance Code 001. The authors also thank the consultant, Dr. Fábio Costa, for providing the human mandibles archives used in the simulations. The research agencies FAPERJ (Projects E26-202.997/2017 and 26/010.001858/2015) and CNPq (Grants 311119/2017-4 and 306141/2019-1) are also acknowledged for their financial support.

6. References

1. Kuntz D, Zhan G-D, Mukherjee AK. Nanocrystalline-matrix ceramic composites for improved fracture toughness. MRS Bull. 2004;29(1):22-7.
2. Basu B. Toughening of yttria-stabilised tetragonal zirconia ceramics. Int Mater Rev. 2005;50(4):239-56.
3. Lange FF. Transformation toughening: part 2 contribution to fracture- toughness. J Mater Sci. 1982;17(1):235-9.
4. Hannink RHJ, Kelly PM, Muddle BC. Transformation toughening in zirconia containing ceramics. J Am Ceram Soc. 2000;83(3):461-87.
5. Chevalier J, Gremillard L, Virkar AV, Clarke DR. The tetragonal-monoclinic transformation in zirconia: lessons learned and future trends. J Am Ceram Soc. 2009;92(9):1901-20.
6. Kisi EH, Kennedy SJ, Howard CJ. Neutron diffraction observations of ferroelastic domain switching and tetragonal-to-monoclinic transformation in Ce-TZP. J Am Ceram Soc. 1997;80(3):621-8.
7. Ma Y, Kisi EH, Kennedy SJ. Neutron diffraction study of ferroelasticity in a 3% mol Y_2O_3–ZrO_2. J Am Ceram Soc. 2001;84(2):399-405.
8. Chevalier J. What future for zirconia as a biomaterial? Biomaterials. 2006;27(4):535-43.
9. Ullman DG. The mechanical design process. New York: McGraw-Hill; 1992. (vol. 2).
10. Sanon C, Chevalier J, Douillard T, Cattani-Lorente M, Scherrer SS, Gremillard L. A new testing protocol for zirconia dental implants. Dent Mater. 2015;31(1):15-25. http://dx.doi.org/10.1016/j.dental.2014.09.002.
11. Janner SF, Gahlert M, Bosshardt DD, Roehling S, Milz S, Higginbottom F, et al. Bone response to functionally loaded, two-piece zirconia implants: a preclinical histometric study. Clin Oral Implants Res. 2018;29(3):277-89..
12. Guo T, Gulati K, Arora H, Han P, Fournier B, Ivanovski S. Orchestrating soft tissue integration at the transmucosal region of titanium implants. Acta Biomater. 2021;124:33-49.
13. Nutu E, Ahmad S, Pastrama S. Influence of bone elastic properties on the predicted stress distribution in the dental implant vicinity. Mater Today Proc. 2017;4(5):5904-8.
14. Piotrowski B, Baptista AA, Patoor E, Bravetti P, Eberhardt A, Laheurte P. Interaction of bone-dental implant with new ultra low modulus alloy using a numerical approach. Mater Sci Eng C. 2014;38:151-60..
15. Yanga J, Xiang H-J. A three-dimensional finite element study on the biomechanical behavior of an FGBM dental implant in surrounding bone. J Biomech. 2007;40(11):2377-85.
16. Misch CE. Dental implant prosthetics. 2nd ed. St Louis: Mosby; 2015. Rationale for dental implants.
17. ASTM: American Society for Testing and Materials. ASTM E1876-15: standard test method for dynamic Young's modulus, shear modulus, and poisson's ratio by impulse excitation of vibration. West Conshohocken: ASTM International; 2015. p. 1-17.
18. ISO: International Organization for Standardization. ISO 6872: dentistry: ceramic materials. Geneva: ISO; 2015.
19. Silva PC, Moreira LP, Alves MFRP, Campos LQB, Simba BG, Santos C. Experimental analysis and finite element modeling of the piston-on-three balls testing of Y-TZP ceramic. Ceramica. 2020;66(377):30-42. http://dx.doi.org/10.1590/0366-69132020663772784.
20. Daguano JKMF. Biovidros e vitrocerâmicos bioativos do sistema $3CaO.P_2O_5$-SiO_2-MgO para aplicações biomédicas: processamento e caracterizações estruturais, mecânicas e biológicas [tese]. Lorena: USP/EEL; 2011.

21. Lin CL, Wang JC, Kuo YC. Numerical simulation on the biomechanical interactions of tooth/implant-supported system under various occlusal forces with rigid/non-rigid connections. J Biomech. 2006;39(3):453-63.
22. Alves MFRP, Ribeiro S, Suzuki PA, Strecker K, Santos C. Effect of Fe_2O_3 addition and sintering temperature on mechanical properties and translucence of zirconia dental ceramics with different Y_2o_3 content. Mater Res. 2021;24(2):e20200402.
23. Amarante JEV, Pereira MVS, Souza GM, Alves MFRP, Simba BG, Santos C. Roughness and its effects on flexural strength of dental yttria-stabilized zirconia ceramics. Mater Sci Eng A. 2019;739:149-57.
24. Matsui K, Yoshida H, Ikuhara Y. Microstructure-development mechanism during sintering in polycrystalline zirconia. Int Mater Rev. 2018;63(6):375-406.
25. Fábregas IO, Reinoso M, Otal E, Kim M. Grain-size/(t ″or c)-phase relationship in dense ZrO_2 ceramics. J Eur Ceram Soc. 2016;36(8):2043-9.
26. Rodrigues J, Martins P. Tecnologia mecânica, tecnologia de deformação plástica. Vol. I - Fundamentos teóricos. 2ª ed. Lisboa: Escolar Editora; 2010. p. 160-3.
27. Young WC, Budynas RG. Roark's formulas for stress and strain. 7th ed. New York: McGraw-Hill; 2002. p. 42-46.
28. Chevalier J, Gremillard L, Virkar AV, Clarke DR. Thetetragonal-monoclinic transformation in zirconia: lessons learned and future trends. J Am Ceram Soc. 2009;92(9):1901-20.
29. Ramesh S, Sara Lee KY, Tan CY. A review on the hydrothermal ageing behaviour of Y-TZP ceramics. Ceram Int. 2018;44(17):20620-34.
30. Abreu LG, Quintino MN, Alves MFRP, Habibe CH, Ramos AS, Santos C. Influence of the microstructure on the life prediction of hydrothermal degraded 3Y-TZP bioceramics. J Mater Res Technol. 2020;9(5):10830-40.
31. Souza RC, Duarte RN, Alves MFRP, Daguano JKMB, Santos C, Strecker K. Cyclic fatigue behaviour of hydrothermally aged 3Y-TZP ceramics in 4-point bending tests. Process Appl Ceram. 2021;15(2):184-94.